photonics

Communication

Understanding Illumination Effect on Saturation Behavior of Thin Film Transistor

Shijie Jiang, Lurong Yang, Chenbo Huang, Qianqian Chen, Wei Zeng and Xiaojian She *

School of Optical Science and Engineering, Zhejiang University, Hangzhou 310027, China
* Correspondence: xjshe@zju.edu.cn

Abstract: Thin film transistor (TFT) has been a key device for planal drive display technology, and operating the TFT device in a saturation regime is particularly important for driving the light emission at a stable current. Considering the light emission reaches the TFT planal, it is thereby meaningful to understand the effect of illumination on TFT saturation behavior in order to improve the stability of light emission. Through experiments and simulations, our study shows that the drift current of photogenerated carriers can follow a saturation behavior when the channel conductance is dominated by charges induced by gate bias rather than the charges generated by photons, and vice versa. The obtained device physics insights are beneficial for developing TFT technologies that can drive light emission at a stable current.

Keywords: thin film transistor; photon charge conversion; charge transport

Citation: Jiang, S.; Yang, L.; Huang, C.; Chen, Q.; Zeng, W.; She, X. Understanding Illumination Effect on Saturation Behavior of Thin Film Transistor. *Photonics* **2023**, *10*, 309. https://doi.org/10.3390/photonics10030309

Received: 18 February 2023
Revised: 7 March 2023
Accepted: 11 March 2023
Published: 13 March 2023

1. Introduction

The thin-film display technology has become increasingly important for both daily usage electronics and industrial electronics [1–4], and has promoted the tremendous development of thin-film transistor (TFT) [5–9]. Over the past decades, tremendous research efforts have been made in the field of light-emitting diodes (LED), and research work through material science and device engineering has contributed greatly to the development of quantum-dot LED [10–13], perovskite LED [14–17] and organic LED [18–21]. Due to the high-quality light emission achieved in these newly developed LED devices, LED display technology has emerged as a key display technology. In each pixel of the LED matrix, a TFT device is integrated to output current for driving the light emission of an LED device. This drive method enables precise control of color intensity by tuning the TFT current via gate bias and has thus been widely used in state-of-art display applications.

During display operation, charge trapping in the LED device would increase its sheet resistance in the TFT-LED circuit, thus resulting in the vibration of voltage applied at the source/drain electrodes of TFT [22–25]. Moreover, the electrostatic charging in the display would also lead to small magnitude vibration of source-drain voltage. Therefore, it is necessary to have the TFT outputting its current in the saturation model where the channel current can retain constant under different source-drain voltages in order to obtain stable light emission. In a practical display application, the light generated from the LED would also reach its neighboring TFT devices. It is known that the electrical characteristics of TFT device are influenced by illumination [26–30]. The photogenerated charges drift within the channel under the control of gate-source-drain biases, coupling with the transistor field-effect current. This has been widely explored in phototransistors mainly for pursuing photodetection and synaptic functionality [31–34], but little has been known about the effect of illumination of the saturation behavior of TFT device that is crucial for TFT-LED applications.

In this work, we investigate pentacene TFT, which is a prototype organic TFT device. We experimentally probe the detail variations of the device's electrical characteristics under illumination and found that the device's saturation behavior is negligibly reduced, which is inspiring for pursuing stable light emission and has not been understood before. We conducted simulation study, and the results show that in devices whose channel conductance is dominated by carriers induced by gate bias rather the photoconductance, the electrical field within the channel under illumination remains the same as that in the dark, and thus the transport of photogenerated carriers in the channel follows the saturation behavior. By contrast, when the photoconductance is largely improved by employing a thick channel or applying high-intensity illumination, the channel conductance would be influenced by the photoconductance, and thereby the photocurrent gradually loses its saturation feature. Our study reveals important device physics insights for pursuing highly stable TFT-driven display technologies.

2. Materials and Methods

2.1. Device Fabrication

A Si/SiO_2 wafer was cut in 15 mm × 15 mm substrates using a laser fragment system, and the highly doped silicon layer and the SiO_2 layer (300 nm) served as the gate electrode and the dielectric layer, respectively. Firstly, the substrates were cleaned by ultrasonic bath in decon 90 (with deionized water), deionized water, acetone and isopropanol for 10 min each. Then the substrates were dried using a nitrogen gun and treated with oxygen plasma for 5 min. Afterwards, the substrates were cleaned again with isopropanol for 5 min. The 2.4 mL Cytop solution was prepared by mixing 0.4 mL Cytop and 2.0 mL solvents in a 7 mL vial. A droplet containing 80 μL Cytop solution was applied to the substrate surface and then immediately a spin-coating process was started at 5000 rpm for 40 s. Thereafter, the substrates were annealed at 100 °C for 10 min in ambient air. Pentacene (purchased from TCI, 99.999%, trace metals basis) was deposited onto the substrate by thermal evaporation to a thickness of 50 nm, at a rate of 0.2 Å/s and under high vacuum of 5×10^{-7} torr, without substrate heating. Finally, an 80 nm gold layer was evaporated through a shadow mask at a rate of 1.0 Å/s and under high vacuum of 1×10^{-6} torr, to serve as the source and drain electrodes. Before measurement, the silicon gate was connected to a gold pad using elargol in nitrogen conditions. The electrical measurements were performed at room temperature in a vacuum probe station (2.0×10^{-4} Torr). All transfer and output characteristics were measured using Keithley 2636B semiconductor analyzer and the kickstart 2 software. The illumination was applied with a white LED light source with an intensity of 100 mW/cm^2. The measurement was conducted by shedding light upon the device through a glass window of the probe station while the device was in a vacuum within the probe station.

2.2. Simulations

In order to have an in-depth investigation of the underlying device physics, we use TCAD tools (Silvaco) to simulate the device operation under illumination. The simulation is based on a package of semiconductor models which includes the Poisson equation, carrier continuity equation, drift-diffusion equation, basic carrier statistics, thermionic emission and general recombination models.

3. Results

The transfer curve and the output curve characteristics of pentacene TFTs were measured under dark and illumination (the light intensity is 100 mW/cm^2), and the data are presented in Figure 1. The results show that there is a photocurrent response at both the off-state region (under the positive gate bias) and the on-state region (under the negative gate bias). To investigate the effect of illumination on the device saturation behavior, we extract the photocurrent ($I_{\mathrm{Photo}} = I_{\mathrm{Light}} - I_{\mathrm{Dark}}$, where I_{Light} and I_{Dark} denote the device current under illumination and dark, respectively) and plot them as a function of drain bias, as shown in Figure 1d. Apparently, it shows that the variation of I_{Photo} is largely reduced at the saturation region where drain bias (V_{D}) is larger than the gate bias (V_{G}), indicating that this photocurrent exhibits a saturation behavior that is typically observed in the transistor output characteristics in the dark (Figure 2c). This is an interesting finding since saturated photocurrent is favorable for maintaining reliable light-emission when charge trapping occurs in the LED device and electrostatic charging occurs in the TFT-LED matrix. Therefore, further investigations were conducted as we want to understand the mechanisms in which photocurrent follows a saturation behavior and the conditions under which it does not.

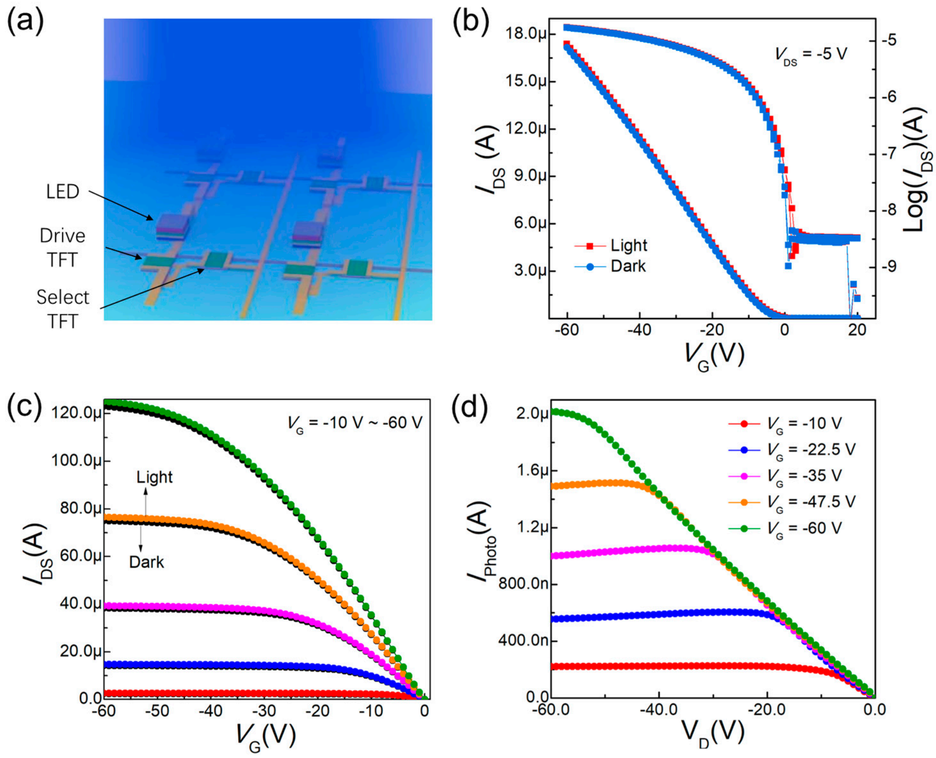

Figure 1. (**a**) Schematic illustration of TFT-LED matrix; (**b**) transfer curve characteristics and (**c**) output characteristics of pentacene TFT measured in dark and illumination; (**d**) photocurrent of the pentacene TFT in the dependence of drain bias.

We have applied simulations to investigate the operation of TFT devices under dark and illumination conditions. To simulate the illumination, we have used a photogeneration rate for the channel. Figure 2 shows the simulation data for transfer curve and output curve characteristics. The results show that the photocurrent response is consistent with the experimental observations discussed above, and the dependence of the characteristics on the photogeneration rate confirms that it originates from photogenerated carriers. As charge injection is a prerequisite for transistor operation, we first investigate the contact resistance (R_C). We extract R_C in the dependence of V_G and injection barrier, as shown in Figure 3a,b. The dependence of R_C on V_G is consistent with reports elsewhere [35]. Additionally, the dependence of R_C (under illumination) on the injection barrier suggests that thermionic charge injection still plays the dominant role in shaping the current continuity at the contact boundary, rather than photogenerated carrier transport, as illustrated in Figure 3d.

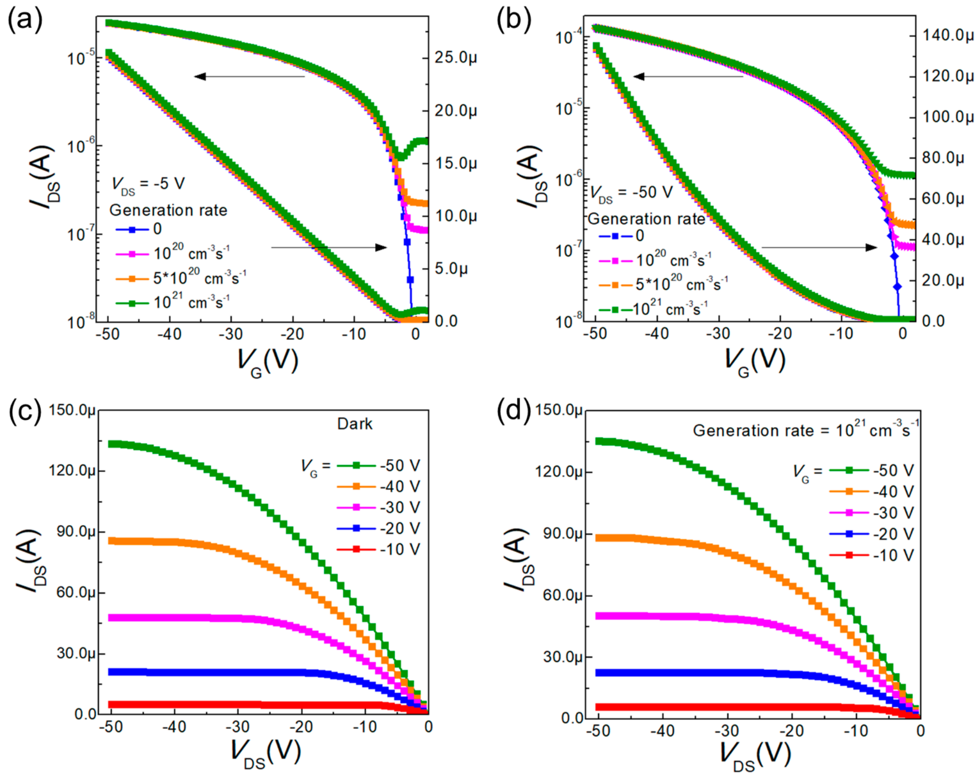

Figure 2. Simulated transfer curve characteristics (**a**,**b**) and output characteristics (**c**,**d**) of a TFT device under various photogeneration rates.

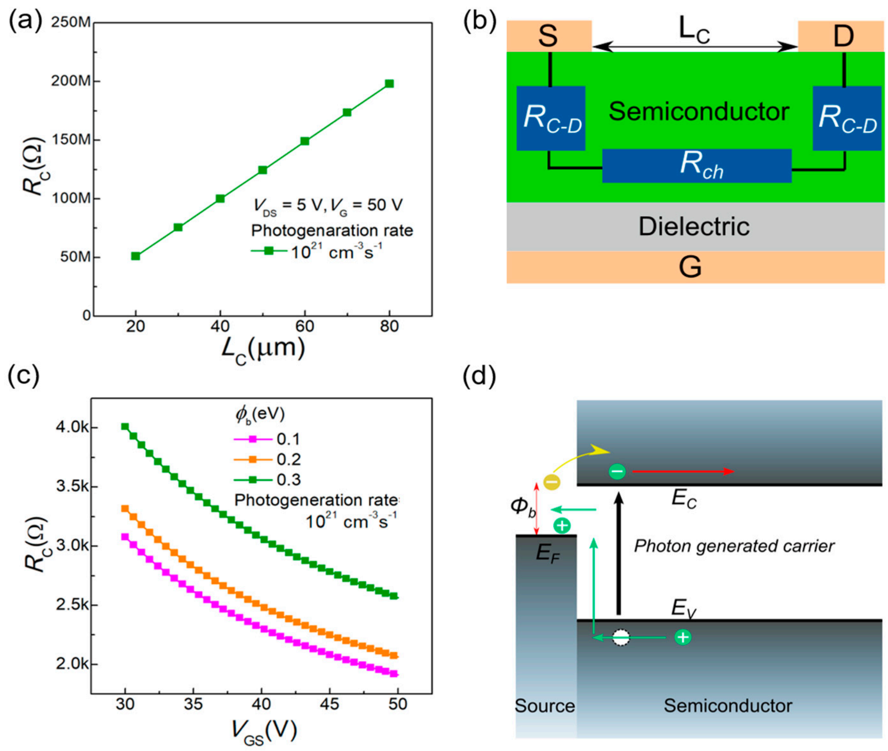

Figure 3. (**a**,**b**) Contact resistance extracted using the TLM method; (**c**) Contact resistance of TFTs with various injection barriers, plotted as a function of gate bias and photogeneration rate; (**d**) illustration of the energy diagram for the charge transport in the contact region. Note that green denotes photogenerated charges, while yellow denotes charges injected from electrodes.

Figure 4c,d show that the extracted I_{Photo} from the simulation data exhibits a saturation behavior that is consistent with the experimental results we discussed above, but we note that the saturation behavior is slightly better. We extract I_{Photo} as a function of the photogeneration rate (5×10^{19}, 1×10^{20}, 1×10^{21} cm^{-3}s^{-1}), as presented in Figure 4a,b. The results show that the saturation feature of I_{Photo} is persistent at different photogeneration rates. To gain further insights, we look at the charge transport by inspecting the surface potential, charge concentration and recombination rate within the channel. Figure 5 presents the surface potential map of TFTs at different drain biases under dark and illumination, while Figure 6 shows the cross-section data of surface potential, charge concentration and recombination rate within the channel under illumination. In the following, we discuss the mechanism of I_{Photo} saturation behavior based on the data in Figures 5 and 6.

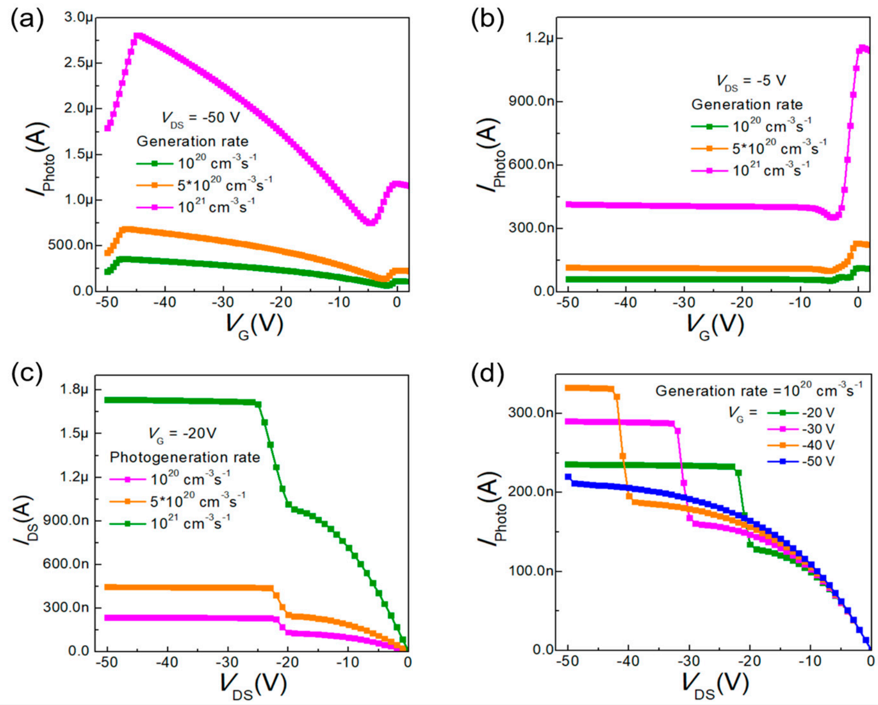

Figure 4. Photocurrent as a function of gate bias (**a**,**b**) and drain bias (**c**,**d**) at different photogeneration rates.

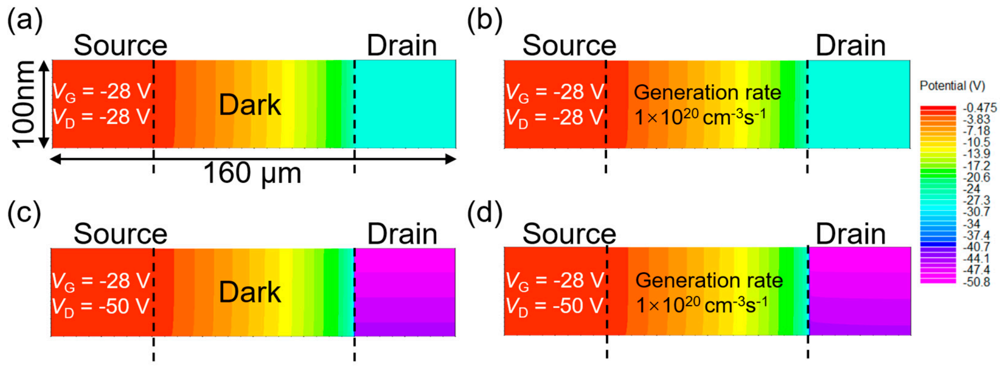

Figure 5. Surface potential mapping in the channel under different bias conditions (V_G = −28 V and V_D = −28 V for (**a**,**b**); V_G = −28 V and V_D = −50 V for (**c**,**d**)) and illumination conditions (Generation rate = 0 for (**a**,**c**); Generation rate = 1×10^{21} cm^{-3}s^{-1} for (**b**,**d**)).

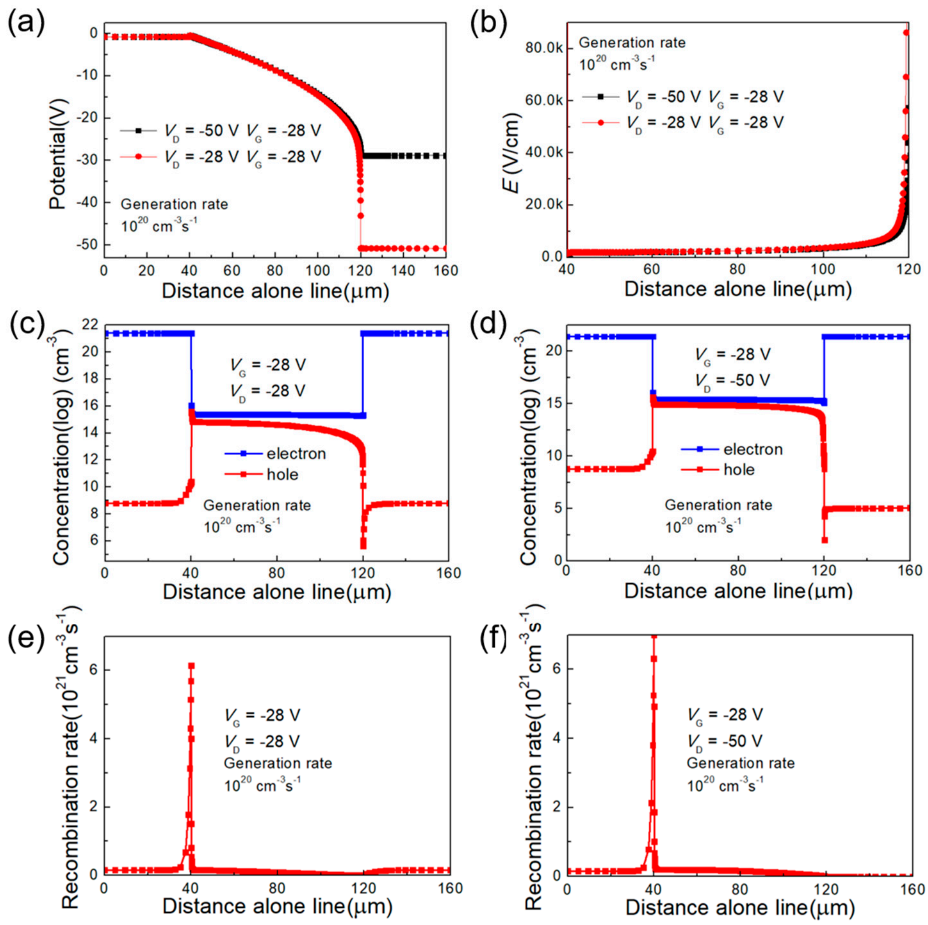

Figure 6. Cross-section data of surface potential (**a**), electrical field (**b**), charge concentration (**c**,**d**) and recombination rate (**e**,**f**) in the channel at different bias conditions under illumination.

We first discuss the spatial photocurrent density in the region between the source electrode and the depletion point, as well as the drain electrode, at the saturation regime. At an illumination with a photogeneration rate of 1×10^{21} cm^{-3}s^{-1} and channel thickness of 100 nm, the areal concentration of photogenerated charge is far below that of carriers induced by gate modulation from the source. Therefore, the channel conductivity is dominated by the conductivity from gate-modulated charges rather than the conductivity from photogenerated charges (termed as photoconductivity). This means that the internal electrical field in this region under illumination is the same as that in the dark condition, as probed by the simulated potential map data in Figure 5. Therefore, the electrical field in this region for driving photogenerated charge is barely changed when altering the drain bias. Furthermore, we note that charge recombination rate is dependent on the charge concentration, which is nearly independent of drain bias in this region since the charge concentration is dominated by the concentration of the gate-modulated charges. This indicates that the recombination rate in this region is nearly independent on drain bias in the saturation regime, as probed by the simulation data in Figure 6. Therefore, with a fixed photogeneration rate, electrical field and recombination rate in this region, the spatial photocurrent density is barely influenced by altering drain bias in the transistor saturation regime.

In addition, we discuss the spatial photocurrent density in the region between the depletion point and the drain electrode in the saturation regime. The cross-section data in Figure 6 show that the electrical field, charge concentration and recombination rate in this region vary when applying different drain biases. Specifically, the electrical field increases when increasing drain bias. However, we note that the increased electrical field accumulates the current cloud, which enlarges the recombination rate in this region, thus decoupling the effect from increased electrical field and contributing to the independence of spatial photocurrent density on drain bias in this region in the saturation regime.

Finally, we extend our investigation to a device with a 1 µm thick channel, and the data are presented in Figure 7. In contrast to the TFT of 100 nm channel, this TFT device shows a photocurrent behavior that has a small saturation feature. The surface potential data show that the electrical field in the channel no longer follows its configuration in the dark condition and varies when changing the drain bias in the saturation regime. This is because the channel conductivity is more influenced by the photoconductivity in a thick channel, and the charge transport in a two-terminal photodiode plays a role. Similarly, the simulation using a high photogeneration rate of up to 1×10^{21} $cm^{-3}s^{-1}$ (simulating high-intensity light illumination) shows that the photocurrent has a small saturated behavior.

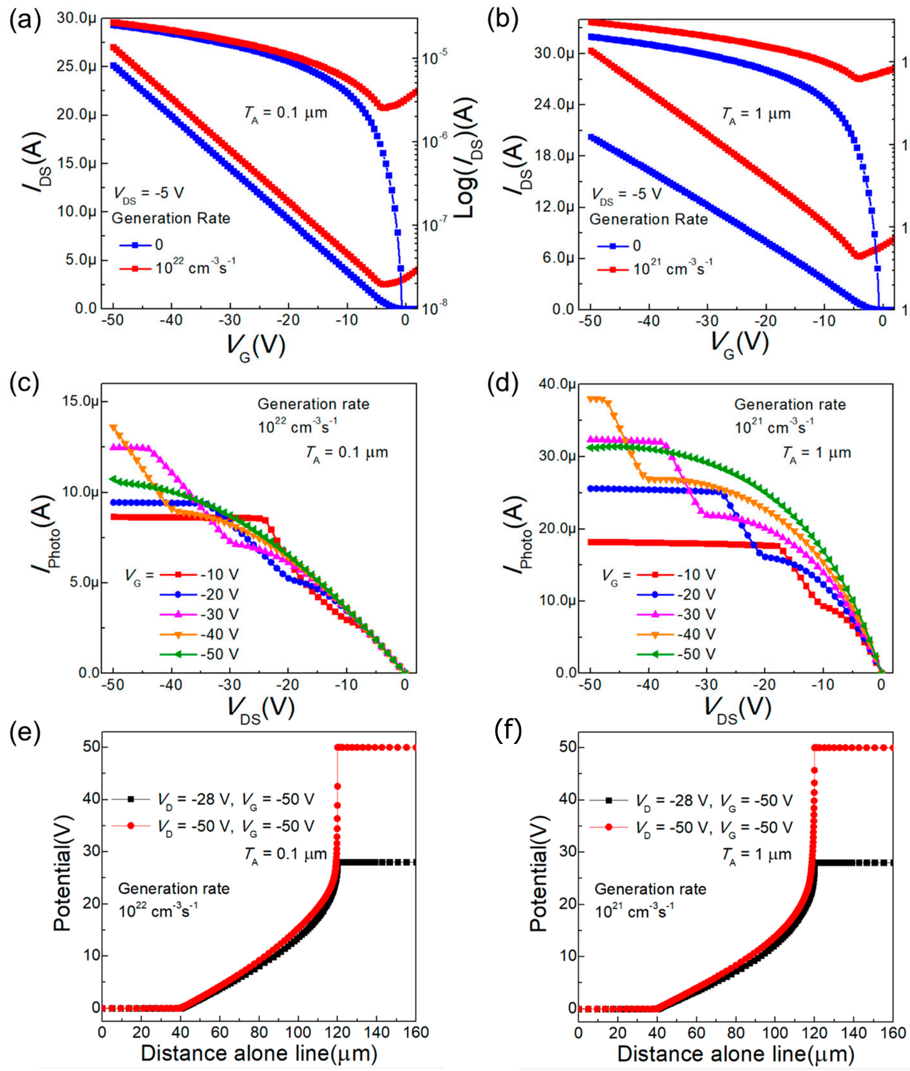

Figure 7. Simulated transfer curve characteristics (**a**,**b**), photocurrent characteristics (**c**,**d**) and cross-section surface potential (**e**,**f**). (**a**,**c**,**e**) are the results of device with 100 nm channel and photogeneration rate of 1×10^{22} $cm^{-3}s^{-1}$; (**b**,**d**,**f**) are the results of device with 1 µm channel and photogeneration rate of 1×10^{21} $cm^{-3}s^{-1}$.

4. Conclusions

In this work, we experimentally investigated the photocurrent saturation behavior in organic thin film transistor and found that the photocurrent saturates in the transistor saturation regime. This discovery is inspiring since it is beneficial for obtaining stable light emission in TFT-LED applications. We conducted simulation investigations to understand the mechanism of saturated photocurrent behavior and the conditions where the photocurrent does not exhibit saturation behavior. The study shows that the interplay between photoconductance and gate-modulated conductance is the key. This device physics insight suggests that having a thin channel layer for the TFT is beneficial for obtaining saturated photocurrent behavior to pursue high-performance and stable light-emitting TFT-LED applications.

Author Contributions: S.J. and L.Y. conducted the experiment. C.H. and X.S. conducted the simulation with in-put from Q.C. and W.Z., X.S. analyzed the data and established the interpretation and supervised the work. All authors wrote and revised the manuscript. All authors have read and agreed to the published version of the manuscript.

Funding: The authors acknowledged the financial support from the Hundred-talents Program of Zhejiang University (No. 1942221R3/005).

Data Availability Statement: The raw data can be accessed upon request from the authors.

Conflicts of Interest: The authors declare no conflict of interest.

References

1. Meng, W.; Xu, F.; Yu, Z.; Tao, T.; Shao, L.; Liu, L.; Li, T.; Wen, K.; Wang, J.; He, L.; et al. Three-Dimensional Monolithic Micro-LED Display Driven by Atomically Thin Transistor Matrix. *Nat. Nanotechnol.* **2021**, *16*, 1231–1236. [CrossRef] [PubMed]
2. Hwangbo, S.; Hu, L.; Hoang, A.T.; Choi, J.Y.; Ahn, J.H. Wafer-Scale Monolithic Integration of Full-Colour Micro-LED Display Using MoS_2 Transistor. *Nat. Nanotechnol.* **2022**, *17*, 500–506. [CrossRef] [PubMed]
3. Kwon, J.Y.; Son, K.S.; Jung, J.S.; Kim, T.S.; Ryu, M.K.; Park, K.B.; Yoo, B.W.; Kim, J.W.; Lee, Y.G.; Park, K.C.; et al. Bottom-Gate Gallium Indium Zinc Oxide Thin-Film Transistor Array for High-Resolution AMOLED Display. *IEEE Electron Device Lett.* **2008**, *29*, 1309–1311. [CrossRef]
4. Xue, Y.; Wang, L.; Zhang, Y.; Liang, G.; Chu, J.; Han, B.; Cao, W.; Liao, C.; Zhang, S. 31-Inch 4K Flexible Display Employing Gate Driver with Metal Oxide Thin-Film Transistors. *IEEE Electron Device Lett.* **2021**, *42*, 188–191. [CrossRef]
5. She, X.J.; Gustafsson, D.; Sirringhaus, H. A vertical organic transistor architecture for fast nonvolatile memory. *Adv. Mater.* **2017**, *29*, 1604769. [CrossRef]
6. Wu, Z.; Liu, Y.; Guo, E.; Darbandy, G.; Wang, S.J.; Hubner, R.; Kloes, A.; Kleemann, H.; Leo, K. Efficient and low-voltage vertical organic permeable base light-emitting transistors. *Nat. Mater.* **2021**, *20*, 1007–1014. [CrossRef]
7. Liu, J.; Zhou, K.; Liu, J.; Zhu, J.; Zhen, Y.; Dong, H.; Hu, W. Organic-single-crystal vertical field-effect transistors and phototransistors. *Adv. Mater.* **2018**, *30*, e1803655. [CrossRef] [PubMed]
8. Jiang, Z.; Zhang, M.; Deng, S.; Yang, Y.; Wong, M.; Kwok, H.-S. Evaluation of positive-bias-stress-induced degradation in InSnZnO thin-film transistors by low frequency noise measurement. *IEEE Electron Device Lett.* **2022**, *43*, 886–889. [CrossRef]
9. Yabuta, H.; Sano, M.; Abe, K.; Aiba, T.; Den, T.; Kumomi, H.; Nomura, K.; Kamiya, T.; Hosono, H. High-mobility thin-film transistor with amorphous InGaZnO4 channel fabricated by room temperature rf-magnetron sputtering. *Appl. Phys. Lett.* **2006**, *89*, 112123. [CrossRef]
10. Dai, X.; Zhang, Z.; Jin, Y.; Niu, Y.; Cao, H.; Liang, X.; Chen, L.; Wang, J.; Peng, X. Solution-Processed, High-Performance light-emitting diodes based on quantum dots. *Nature* **2014**, *515*, 96–99. [CrossRef]
11. Shirasaki, Y.; Supran, G.J.; Bawendi, M.G.; Bulović, V. Emergence of colloidal quantum-dot light-emitting technologies. *Nat. Photonics* **2012**, *7*, 13–23. [CrossRef]
12. Caruge, J.M.; Halpert, J.E.; Wood, V.; Bulović, V.; Bawendi, M.G. Colloidal quantum-dot light-emitting diodes with metal-oxide charge transport layers. *Nat. Photonics* **2008**, *2*, 247–250. [CrossRef]
13. Kirkwood, N.; Singh, B.; Mulvaney, P. Enhancing quantum dot led efficiency by tuning electron mobility in the zno electron transport layer. *Adv. Mater. Interfaces* **2016**, *3*, 1600868. [CrossRef]
14. Hassan, Y.; Park, J.H.; Crawford, M.L.; Sadhanala, A.; Lee, J.; Sadighian, J.C.; Mosconi, E.; Shivanna, R.; Radicchi, E.; Jeong, M.; et al. Ligand-Engineered Bandgap Stability in Mixed-Halide Perovskite LEDs. *Nature* **2021**, *591*, 72–77. [CrossRef]
15. Cheng, L.; Jiang, T.; Cao, Y.; Yi, C.; Wang, N.; Huang, W.; Wang, J. Multiple-Quantum-Well Perovskites for High-Performance Light-Emitting Diodes. *Adv. Mater.* **2020**, *32*, 1904163. [CrossRef]
16. Cao, Y.; Wang, N.; Tian, H.; Guo, J.; Wei, Y.; Chen, H.; Miao, Y.; Zou, W.; Pan, K.; He, Y.; et al. Perovskite Light-Emitting Diodes Based on Spontaneously Formed Submicrometre-Scale Structures. *Nature* **2018**, *562*, 249–253. [CrossRef] [PubMed]
17. Lin, K.; Xing, J.; Quan, L.N.; de Arquer, F.P.G.; Gong, X.; Lu, J.; Xie, L.; Zhao, W.; Zhang, D.; Yan, C.; et al. Perovskite Light-Emitting Diodes with External Quantum Efficiency Exceeding 20 per cent. *Nature* **2018**, *562*, 245–248. [CrossRef]
18. Hong, G.; Gan, X.; Leonhardt, C.; Zhang, Z.; Seibert, J.; Busch, J.M.; Brase, S. A Brief History of OLEDs-Emitter Development and Industry Milestones. *Adv. Mater.* **2021**, *33*, 2005630. [CrossRef]

19. Kang, C.-m.; Lee, H. Recent Progress of Organic Light-Emitting Diode Microdisplays for Augmented Reality/Virtual Reality Applications. *J. Inf. Disp.* **2021**, *23*, 19–32. [CrossRef]
20. Luo, Y.; Li, S.; Zhao, Y.; Li, C.; Pang, Z.; Huang, Y.; Yang, M.; Zhou, L.; Zheng, X.; Pu, X.; et al. An Ultraviolet Thermally Activated Delayed Fluorescence OLED with Total External Quantum Efficiency over 9%. *Adv. Mater.* **2020**, *32*, 2001248. [CrossRef] [PubMed]
21. Kondo, Y.; Yoshiura, K.; Kitera, S.; Nishi, H.; Oda, S.; Gotoh, H.; Sasada, Y.; Yanai, M.; Hatakeyama, T. Narrowband Deep-Blue Organic Light-Emitting Diode Featuring an Organoboron-based Emitter. *Nat. Photonics* **2019**, *13*, 678–682. [CrossRef]
22. Zhang, Z.; Wang, W.; Jiang, Y.; Wang, Y.X.; Wu, Y.; Lai, J.C.; Niu, S.; Xu, C.; Shih, C.C.; Wang, C.; et al. High-Brightness All-Polymer Stretchable LED with Charge-Trapping Dilution. *Nature* **2022**, *603*, 624–630. [CrossRef]
23. Wang, Q.; Ding, J.; Ma, D.; Cheng, Y.; Wang, L.; Jing, X.; Wang, F. Harvesting Excitons Via Two Parallel Channels for Efficient White Organic LEDs with Nearly 100% Internal Quantum Efficiency: Fabrication and Emission-Mechanism Analysis. *Adv. Funct. Mater.* **2009**, *19*, 84–95. [CrossRef]
24. Diethelm, M.; Bauer, M.; Hu, W.H.; Vael, C.; Jenatsch, S.; Blom, P.W.M.; Nüesch, F.; Hany, R. Electron Trap Dynamics in Polymer Light-Emitting Diodes. *Adv. Funct. Mater.* **2022**, *32*, 2106185. [CrossRef]
25. Kuik, M.; Wetzelaer, G.J.; Nicolai, H.T.; Craciun, N.I.; De Leeuw, D.M.; Blom, P.W. 25th Anniversary Article: Charge Transport and Recombination in Polymer Light-Emitting Diodes. *Adv. Mater.* **2014**, *26*, 512–531. [CrossRef] [PubMed]
26. Jing, B.; Peng, C.; Xu, M.; Huang, H.; Li, X.; Zhang, J. Investigation on Stability in Solution-Processed In-Zn-Sn-O TFT Array Under Various Intensity of Illumination. *IEEE Trans. Electron Devices* **2022**, *69*, 4283–4287. [CrossRef]
27. Billah, M.; Chowdhury, M.; Mativenga, M.; Um, J.; Mruthyunjaya, R.; Heiler, G.; Tredwell, T.; Jang, J. Analysis of Improved Performance Under Negative Bias Illumination Stress of Dual Gate Driving a- IGZO TFT by TCAD Simulation. *IEEE Electron Device Lett.* **2016**, *37*, 735–738. [CrossRef]
28. Lin, Y.-J.; Huang, B.-C. Influence of Illumination on the Output Characteristics in Pentacene Thin Film Transistors. *Mater. Chem. Phys.* **2013**, *142*, 428–431. [CrossRef]
29. Xiong, N.; Xiao, P.; Li, M.; Xu, H.; Yao, R.; Wen, S.; Peng, J. Enhancement of Bias and Illumination Stability in Thin-Film Transistors by Doping In ZnO with Wide-Band-Gap Ta_2O_5. *Appl. Phys. Lett.* **2013**, *102*, 242102. [CrossRef]
30. Kim, S.G.; Kim, S.H.; Park, J.; Kim, G.S.; Park, J.H.; Saraswat, K.C.; Kim, J.; Yu, H.Y. Infrared Detectable MoS_2 Phototransistor and Its Application to Artificial Multilevel Optic-Neural Synapse. *ACS Nano* **2019**, *13*, 10294–10300. [CrossRef]
31. Li, P.; Zhang, X.; Chong, W.C.; Lau, K.M. Monolithic Thin Film Red LED Active-Matrix Micro-Display by Flip-Chip Technology. *IEEE Photonics Technol. Lett.* **2021**, *33*, 603–606. [CrossRef]
32. Zhang, Q.; Jin, T.; Ye, X.; Geng, D.; Chen, W.; Hu, W. Organic Field Effect Transistor-Based Photonic Synapses: Materials, Devices, and Applications. *Adv. Funct. Mater.* **2021**, *31*, 2106151. [CrossRef]
33. Baeg, K.J.; Binda, M.; Natali, D.; Caironi, M.; Noh, Y.Y. Organic Light Detectors: Photodiodes and Phototransistors. *Adv. Mater.* **2013**, *25*, 4267–4295. [CrossRef] [PubMed]
34. Han, T.; Sun, L.; Feng, Q.; Cao, K.; Ding, S.; Jin, G.; Jiang, C.; Huang, X. The Mechanism of Photogenerated Minority Carrier Movement in Organic Phototransistors. *J. Mater. Chem. C* **2020**, *8*, 12284–12290. [CrossRef]
35. Wang, S.D.; Yan, Y.; Tsukagoshi, K. Understanding contact behavior in organic thin film transistors. *Appl. Phys. Lett.* **2010**, *97*, 063307. [CrossRef]